Numerical simulation of multicomponent diesel fuel spray surrogates using real-fluid thermodynamic modelling

Author, co-author (Do NOT enter this information. It will be pulled from participant tab in MyTechZone)

Affiliation (Do NOT enter this information. It will be pulled from participant tab in MyTechZone)

Abstract

Computational models widely employed for predicting the dispersion of fuel sprays in combustion engines suffer from well-known drawbacks associated with the utilization of case-dependent empirical phase-change models, describing the conversion of liquid into vapour during fuel injection. The present work couples the compressible Navier-Stokes and energy conservation equations with a thermodynamic closure approximation covering pressures from 0 to 2000bar and temperatures that expand from compressed liquid, vapor-liquid equilibrium to trans/supercritical mixing, and thus, cover the whole range of P-T values that diesel fuel undergoes during its injection into combustion engines. The model assumes mechanical and thermal equilibrium between the liquid, vapour and surrounding air phases and thus, it avoids utilization of case-dependent empirical phase-change models for predicting in-nozzle cavitation and vaporization of fuels. Model development is based on the recent works reported for one mono-component (*n*-dodecane) and extended here to consider the influence of two multicomponent diesel surrogates. Fuel properties are predicted via the Perturbed Chain Statistical Associating Fluid Theory (PC-SAFT) equation of state (EoS). The tabulated thermodynamic approach proposed is based on P-T tables, providing very high accuracy across the range of conditions with only a small number of interpolation points. The developed model is validated against experimental data for the liquid and vapour penetration for the Spray A conditions reported in the Engine Combustion Network (ECN) database. Results show good agreement for three non-reacting target conditions. Then, from simulations obtained using the two multi-component fuel surrogates their effect can be quantified on spray development.

Introduction

Diesel fuel is composed of hundreds of hydrocarbon molecules; the principal chain could have predominantly 9 to 20 carbon atoms [1],while the final composition is directly linked to the oil source and refinement process [2]. In addition, commercial diesel fuel contains small amounts of sulphur, nitrogen, oxygen, which provide natural lubrication and reducing wear of the fuel injection equipment. It could also contain other additives to adjust its performance characteristics as dispersants, detergents and anti-freezing molecules [3].

These broad variations make it impractical to use real fuel composition in both numerical simulations and in some experimental tests in order to ensure comparable properties and reproducibility [4].To evaluate the influence of diesel fuel composition, surrogates are used to emulate the physical and chemical properties of a target-diesel fuel. The effectiveness of multicomponent diesel surrogates to represent diesel fuel is easier to be tested experimentally; however, their utilization in numerical simulations imposes more challenges [5]. These reside on the reproduction of physical and chemical properties and component interactions, which is normally linked with the increase of the model computational cost.

The most common surrogate to emulate diesel fuel properties is n-dodecane [6]. Even though it does not fully cover the complexity of diesel fuel composition, it provides a reasonable approximation and is broadly used in a wide range of applications [7]. In a more refined approach, the diesel fuel composition can be grouped by considering four main hydrocarbon classes: n-alkanes, iso-alkanes, cyclo-alkanes and aromatics [4,8-9].

Pei *et al.* [10] used a binary mixture for a diesel surrogate, including the aromatic class of hydrocarbons. This surrogate was composed of n-dodecane and m-xylene and its skeletal chemical mechanism was validated against both the detail chemical mechanism and the relevant experimental data. Sun *et al.* [11] used a ternary mixture of 2,2,4,4,6,8,8-Heptamethylnonane (HMN),1-Methylnaphthalene and n-Hexadecane to model the properties of No.2 diesel. They validated the surrogate's performance against the ECN Spray A numeric simulations. Qian *et al.* [12] proposed three surrogates distinguished by varying the number of their components: 3-components (n-hexadecane, HMN,1-methylnaphthalene), 5-components (n-hexadecane, n-octadecane, HMN, 1-methylnaphthalene, decalin) and 7-components (n-hexadecane, n-octadecane, HMN, 1-methylnaphthalene, decalin, n-butylbenzene, n-butylcyclohexane). These surrogates were tested in terms of their effectiveness to represent engine performance and emissions.

Recently, Sun *et al.*[13]developed a four-component surrogate for marine diesel applications composed of n-tetradecane, toluene, methylcyclohexane and ethanol. Their derivate chemical mechanism was validated against measurements obtained in a shock tube, in a counterflow configuration and a marine engine. Mueller *et al.* [14] used a regression model to compose a four surrogate formulation and characterized those formulations against the compositional characteristics of the no. 2-D S15 diesel. These have been classified

as lower- and higher-compositional-accuracy diesel surrogate fuels, depending on the number of components; the first group contains four and fine components (indicated as V0a and V0b, respectively) and the second eight and nine components (indicated as V1 and V2, respectively).

Additional complexities in the simulation of the physical properties of fuel surrogates exist when considering their variation with pressure and temperature that expand beyond the critical point of the Diesel fuel [15]. In those conditions, compressibility effects become relevant and the use of constant properties in those cases lead to significant inaccuracies [16]. Besides, the relative importance of shear and surface tension forces during fuel atomization and evaporation under trans- and supercritical conditions is not significant; fuel mixing is governed by supercritical diffusion [15,17].

In order to capture those phenomena, real-fluid equations of state (EoS) need to be considered. Previously reported most common EoS such as the cubic EoS, like the Soave-Redlich-Kwong (SRK)[18] and the Peng-Robinson [19] were largely applied, despite their compromised accuracy [20]. Their conception is based only on van der Wall dispersion forces [21], as a consequence, their precision decreases at conditions of strong association between molecules and at high pressure and high temperature (HPHT) conditions [22,23]. Recent works from the author's group report measurements and validated modelling methods predicting the variation of diesel fuel properties at pressures as high as 3000bar and temperatures up to approximately 550K [24-33].

An alternative is the utilization of the Statistical Associating Fluid Theory (SAFT) molecular where the residual Helmholtz free energy and the perturbation theory are taken into account [34]. Among the variants of the SAFT model, the Perturbed-Chain (PC-SAFT) EoS is the most notable variation; the Helmholtz free energy contribution is applied to hard spheres [35]. In general, the PC-SAFT EoS predictions are more accurate with regards to thermodynamics and transport fuel properties in comparison to cubic EoS [36], especially in multicomponent mixture [37-39]. In contrast, cubic EoS are computationally efficient [40]. In order to reduce the calculations time and save computational cost, tabulated methods are common techniques applied on fluid dynamic simulations [41-42].

In recent work of the author's group, the PC-SAFT EoS has been coupled with a fluid flow solver in order to simulate a transcritical jet [43-44], as well as a Spray A injection, also combined with machine learning [45]. However, both of these studies use a single component surrogate, n-dodecane, instead of the multi-component mixtures mentioned above. In another study by the group [46], a multi component surrogate is used for the simulation of cavitating in-nozzle flow. However, in this case no comparison with experimental data is done, in order to evaluate the overall precision of this coupled methodology for multi component mixtures.

As the discursion above reveals, the effect of using realistic surrogates and their modelling is a complex area, especially for computationally efficient simulations in practical applications. The overarching goal of this study is to understand the sensitivity of CFD predictions on the selection of fuel surrogate under the conditions of the non-reactive ECN Spray A. Therefore, the main objectives of this study are: (i) to validate the computational methodology against measurements of liquid and vapour penetration; (ii) to apply this approach to more complex surrogates without a significant increase of the computational cost; (iii) to demonstrate the differences when considering the multi-component fuel surrogates on diesel spray development.

Numeric method

The compressible form of the Navier-Stokes and energy conservation equations are solved numerically using the commercial pressure-based solver, Fluent v19.1 [47]; the flow solver is supplemented with external user-defined functions (UDFs) to incorporate the variation of the physical and transport properties of the liquid, vapor and air as function of pressure and temperature. Numerical simulations are performed in a two-dimensional axisymmetric configuration. The fuel and air are treated as homogeneous mixture under mechanical and thermal equilibrium; as a consequence, all phases and components share the same velocity, pressure and temperature fields in each computational cell. In addition, a diffuse-interface approximation is assumed at the liquid-air interface. The four-equation model utilized is:

$$\frac{\partial \rho}{\partial t} + \nabla \cdot (\rho \vec{v}) = 0 \tag{1}$$

$$\frac{\partial}{\partial t}(\rho \vec{v}) + \nabla \cdot (\rho \vec{v}\vec{v}) = -\nabla p + \nabla \cdot (\bar{\bar{\tau}}) \tag{2}$$

$$\frac{\partial \rho_l y_{fuel}}{\partial t} + \nabla \cdot \left(\rho_l \vec{v}_l y_{fuel}\right) = -\nabla \vec{J} \tag{3}$$

$$\frac{\partial \rho E}{\partial t} + \nabla \cdot [v(\rho E + p)] = \nabla \cdot \left(\left(k_{eff} \nabla T\right) + (h\vec{J}) + \left(\bar{\bar{\tau}}_{eff} \cdot \vec{v}\right)\right) \tag{4}$$

where ρ is the mixture density, $\vec{v}$ is the velocity vector field, p is the pressure, y_{fuel} is the fuel mass fraction, E is the total energy, k_{eff} is the total effective thermal conductivity, T is the temperature, h is the enthalpy, the viscous stress tensor $\bar{\bar{\tau}} = \mu[(\nabla \vec{v}) + \nabla \vec{v}^T]$, with μ being the dynamic viscosity and k_{eff} is the total effective thermal conductivity.

The mass diffusion flux, $\vec{J}$, is based on the dilute approximation and can be defined as:

$$\vec{J} = -\left(\rho D_m + \frac{\mu_t}{Sc_t}\right) \nabla y_{fuel} - D_T \frac{\nabla T}{T} \tag{5}$$

were μ_t is the turbulent viscosity, D_m is the mass diffusion coefficient for species in the mixture, D_T is the thermal (Soret) diffusion coefficient and Sc_t correspond to the turbulent Schmidt number $Sc_t = \frac{\mu_t}{\rho D_t}$, where D_t is the turbulent diffusivity. The diffusion coefficients are calculated using the kinetic theory and the parameters needed are based on the work of Tahery and Modarress [48]. Table 1 shows the values used.

Table 1: Kinetic theory parameters for the surrogates

	σ [Å]	ε/kB [K]
n-dodecane	7.58	622.51
V0a	8.2390	696.6401
V1	8.0830	680.311

Turbulence closure is achieved by employing the Reynolds Averaged Navier-Stokes (RANS) approach with the standard $k-\varepsilon$ model:

$$\frac{\partial \rho k}{\partial t} + \nabla \cdot (\rho \vec{v} k) = \nabla \cdot \left[\left(\mu + \frac{\mu_t}{\sigma_k}\right) \nabla k\right] + G_k + \rho\varepsilon - Y_M \quad (6)$$

$$\frac{\partial \rho \varepsilon}{\partial t} + \nabla \cdot (\rho \vec{v} \varepsilon) = \nabla \cdot \left[\left(\mu + \frac{\mu_t}{\sigma_\varepsilon}\right) \nabla \varepsilon\right] + C_{1\varepsilon} \frac{\varepsilon}{k} G_k - C_{2\varepsilon} \rho \frac{\varepsilon^2}{k} \quad (7)$$

where G_k represents the generation of turbulence kinetic energy due to the mean velocity gradients, Y_M represents the contribution of the fluctuating dilatation in compressible turbulence to the overall dissipation rate, $C_{1\varepsilon}, C_{2\varepsilon}$ are constants, σ_k σ_ε are the turbulent Prandtl numbers for turbulence kinetic energy k and its rate of dissipation ε. All parameters are kept with the default values, except for the Schmidt number and C1. These two parameters were adjusted respectively to 0.5 and 1.52, based on [49].

The discretization of the governing equations is done with a second order upwind scheme, except for the transport equation and mass diffusion flux of the fuel. In those equations, the QUICK (Quadratic Upwind Interpolation for Convective Kinematics) and Third Order Upwind have been used, respectively.

Thermodynamic properties

The thermodynamic properties of the fuel and ambient gas are calculated using the PC-SAFT EoS and Vapor Liquid Equilibrium (VLE) calculations. In the PC-SAFT a reference fluid is defined to calculate the repulsive contribution. The reference fluid is composed of spherical segments comprising a hard sphere fluid that then forms molecular chains to create the hard-chain fluid. The attractive interactions, perturbations to the reference system, are accounted for with the dispersion term [35]. The final expression of the residual Helhomtz free energy is defined as:

$$a_{res} = a_{hc} + a_{disp} \quad (8)$$

The detailed expression of these terms is rather lengthy; thus, the interested reader is addressed to the original publication of the model [35]. All thermodynamic properties can be defined as functions of the residual Helmholtz energy and its derivatives. The transport properties are estimated using the residual entropy scaling method, presented in [50] for dynamic viscosity and [51] for thermal conductivity. The VLE calculations are done at constant pressure and temperature and consist of two parts. First the mixture is assumed to be in a single-phase state and its stability is investigated through the Tangent Plane Distance [52]. Then the algorithm proceeds with the TP flash calculations, the minimization of the Gibbs Energy under constant pressure and temperature, as presented in [53]. Through the flash calculations the composition of the liquid and vapor phase is calculated, as well as the vapor molar fraction.

Both parts of this code can be seen as optimization problems. The stability problem is solved using the quasi-Newton Method BFGS (Broyden-Fletcher-Goldfarb-Shanno). For the flash problem a BFGS is used, together with a classical Newton-Raphson minimization method for the Rachford-Rice, based on the algorithm of [53].

All calculations are done in advance and the thermodynamic and transport properties are stored in structured 3D tables. These can then be accessed by the CFD code using a combination of pressure, temperature and fuel mass fraction to updated the fuel/gas properties inside each computational cell.

Simulation configuration and cases setup

The Spray A injector is a single-hole, common rail, Bosch solenoid-activated diesel injector extensively utilized in ECN. Applied at HPHT evaporating conditions, Spray A injector has a nominal nozzle outlet diameter of 0.090mm, orifice length of 1mm and a k-factor of 1.5. The computational domain consists of the nozzle's sac volume, the nozzle hole orifice and the combustion chamber downstream of the nozzle hole exit; this extents 50mm in the axial and 15mm in the radial directions, respectively. The exact hole radius variation along the injector axis is available at the ECN website [54].

The computational grid utilized body-fitted quadrilateral cells. The injection hole is discretized with 20 cells in the radial direction, corresponding to a resolution of 2 μm. Moving at distances further away from the nozzle exit, the mesh becomes coarse with a maximal size of 0.6mm. This refinement strategy is based on previous validated study published by the author [55] and results in a mesh of 49k cells with a maximum y+ of ~50.

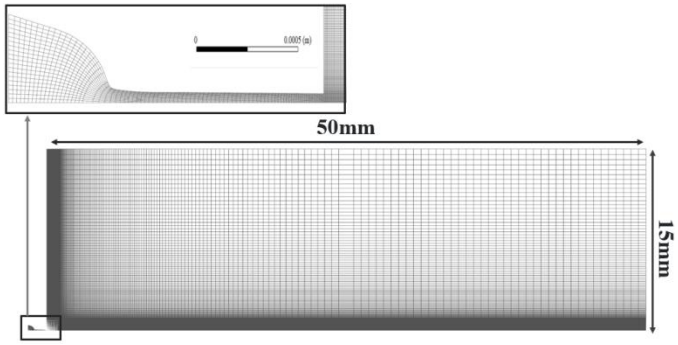

Figure 1. The computational mesh used for the reported simulations

The base line cases have been conducted with pure *n*-dodecane (*n*-$C_{12}H_{26}$) as fuel and the boundary conditions are chosen based on the experimental data at inert conditions (0% oxygen) available on the ECN website [56]. To ensure the non-reacting condition in the numerical simulations, the chamber is initialized with only nitrogen (N_2), at three fixed pressure and temperature conditions and zero gradient for all other quantities: 60bar and 900k; 50bar and 1100k; 30bar and 1400k. Details of the downstream condition are given in Table 2.

Table 2. Ambient conditions for Spray A

Case	Pressure [bar]	Temperature [K]	Density [Kg/m^3]
#1	60	900	22.8
#2	50	1100	15.2
#3	30	1400	7.5

In addition to *n*-dodecane base line cases, a comparison of different fuel surrogates in the same cases has been carried out. The fuels were chosen to highlight the compositional difference between *n*-dodecane and the selected surrogates V0a and V1. The V0a is composed of four components and V1 is composed of nine components. Tables 3 and 4 provide the fuel molar composition and properties of the three surrogates [14,57-58].

Table 3: Fuel composition for Diesel surrogates [14]

Compound	Molar comp. [g/mol]	Boiling point [K]	Surrogate mol %		
			n-C12H26	V0a	V1
dodecane	170.3	489.0	100	-	-
n-hexadecane	226.4	560.0	-	27.8	2.7
n-octadecane	254.5	590.0	-		20.2
heptamethylnonane	226.4	520.0	-	36.3	29.2
n-butylcyclohexane	140.3	456.2	-	-	5.1
trans-decalin	138.2	460.5	-	14.8	5.5
1.2.4-trimethylbenzene	120.2	442.6	-	-	7.5
tetralin	132.2	480.9	-	-	15.4
1-methylnaphthalene	142.2	518.0	-	21.1	14.4

* Boiling points at 0.10MPa

Table 4: Fuel properties [14,59]

	n-C12H26	V0a	V1
Density [Kg/m^3]	750	818	828.4
Flash point (°C)	74	88	83
Kinematic viscosity (cSt)	1.99	2.452	2.303

The injection conditions (1500bar and fuel temperature of 363K) are kept constant in all numerical simulations. Additionally, the nozzle walls are considered adiabatic. The inlet boundary condition is based on the measured mass flow rate profile. This profile is reported in [60] as function of injection pressure, ambient back pressure, fuel density, injector nominal parameters and injection duration. The curves used are depicted in Figure 2.

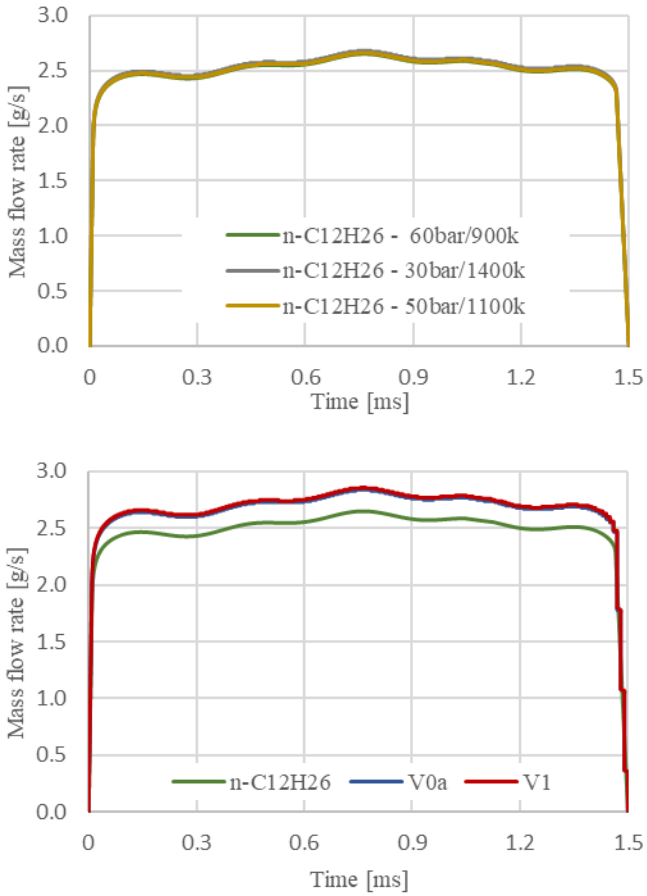

Figure 2: Mass flow rate: (a) n-dodecane at different ambient conditions; (b) different surrogates at 900K and 22.8kg/m^3 ambient condition.

All simulations are carried out for 1.5ms simulation time, in a workstation within 12 cores; 4.1 hours of CPU time is required for each case.

Results

Spray A validation

First, the model is validated using n-dodecane as liquid fuel for three ambient conditions: 900K and 22.8kg/m^3 (60bar), 1100K and 15.2kg/m^3 (50bar), 1400K and 7.6kg/m^3 (30bar). The main objective of the validation at three different ambient conditions is to confirm the extension and capabilities of the aforementioned tabulate approach. Figure 3 shows the temporal evolution of the vapor penetration along with the experimental data [61]. Here, the vapor penetration is defined, according ECN guidelines, as 0.1% of the vapor concentration at the maximal axial distance. Vapor penetration is inversely proportional to the ambient density. At higher density (22.8kg/m^3) the fuel presents the lowest vapor penetrations and at 7.6kg/m^3 the highest one. Also, at density values of 15.2kg/m^3 and 7.6kg/m^3, the numerical results slightly overestimate the experimental ones. Nevertheless, both results can be considered satisfactory.

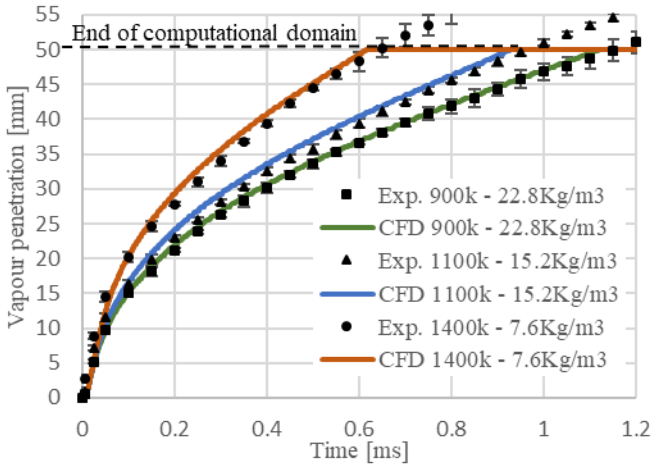

Figure 3: Vapor penetration of n-dodecane for three downstream conditions.

The numerical results of liquid penetration are also compared against the experimental data [61] in Figure 4. Between 0.05 and 0.01ms a steep increase on the liquid penetration is observed, surpassing the experimental results and followed by an instant drop that follows the expected trend in following times. This temporary overestimation is consequence of the detachment of a small part of the liquid core, which vaporizes fast [62]. It is important to emphasize that the experimental liquid penetration is estimated based on the liquid core length, identified following the ECN guidelines, based on the distance of the iso-surface of 0.15% liquid volume fraction. Thereby, after the initial liquid detachment from the main core, liquid penetration shows a satisfactory agreement with the experimental data uncertainty in all cases.

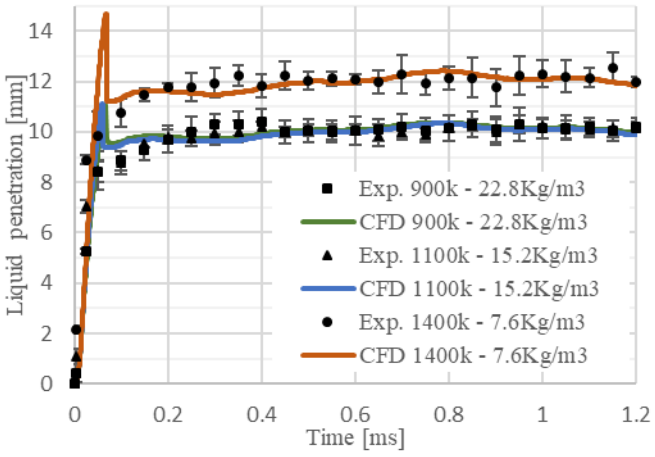

Figure 4: Liquid penetration of n-dodecane for three downstream conditions.

Figures 5 and 6 show the *n*-dodecane mass fraction distribution profiles against the experimental data reported in [61] for 900K and 22.8kg/m^3, and 1100K and 15.2kg/m^3, respectively. For the 1400K and 7.6kg/m^3 case, mass fraction and temperature distribution along the jet central line were not available. In both cases, the mass fraction distributions are well predicted for all axial distances.

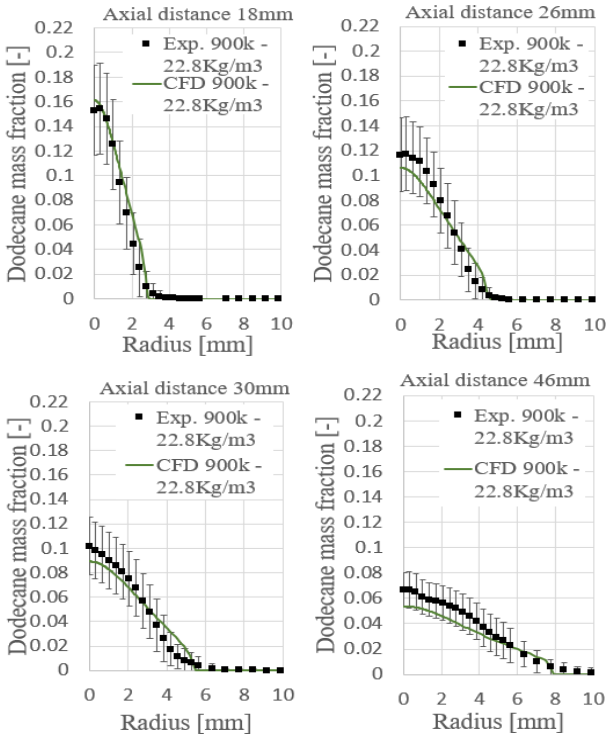

Figure 5: Radial profiles of mixture fraction of n-dodecane at different distances from the nozzle exit, at 900K and 22.8kg/m^3 ambient conditions.

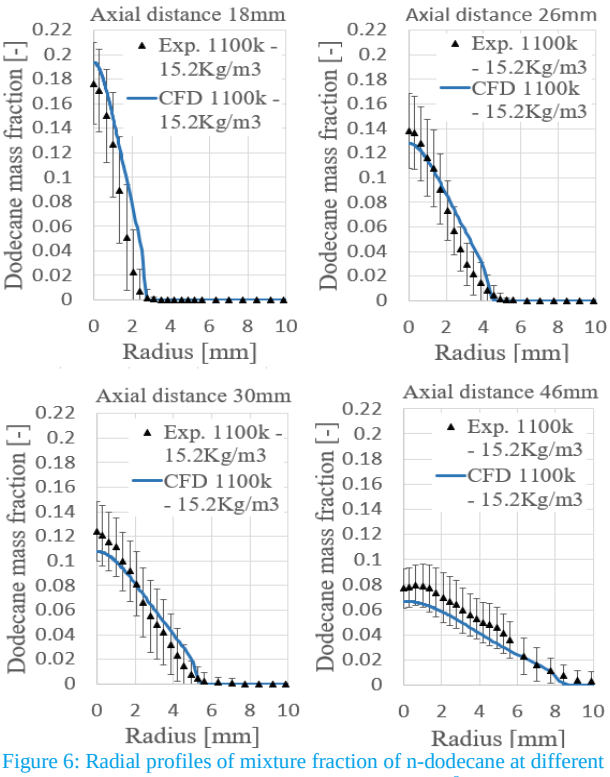

Figure 6: Radial profiles of mixture fraction of n-dodecane at different distances from the nozzle exit at 900K and 22.8kg/m^3 ambient conditions.

Finally, predictions for temperature variation along the spray centre-line are compared against the experimental data of [61] in Figure 7. Overall, the numerical predictions are in close agreement with the measurements.

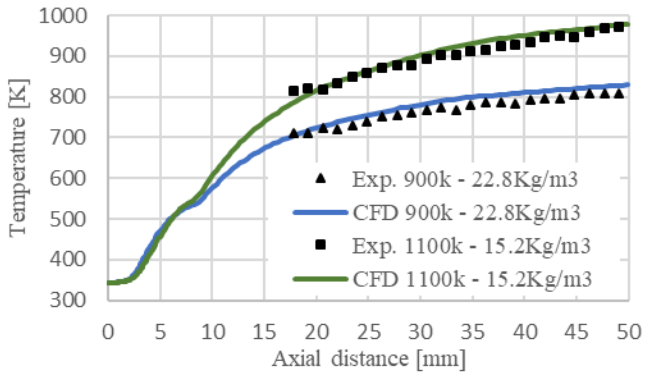

Figure 7: Temperature distribution along the jet centreline for two downstream conditions.

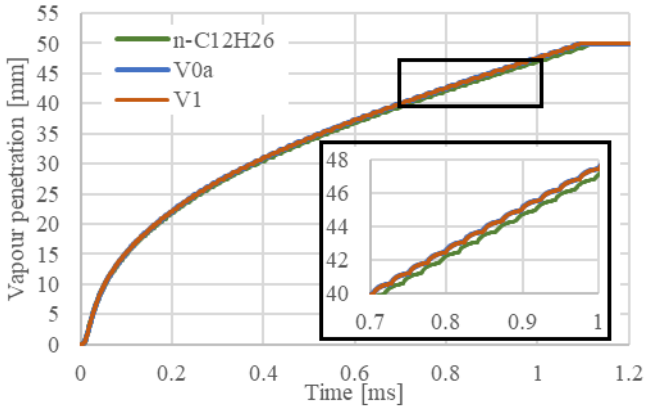

Figure 8: Vapor penetration for n-dodecane, V0a and V1 at 900K and 22.8kg/m^3 ambient condition.

Summarizing, it can be claimed that the simulations exhibit satisfactory prediction of the experimental data in all conditions analyzed, demonstrating the versatility of the employed numerical methodology. It can be noted that in complement to the previous study from the authors [55], the range of applicability of the tabulated thermodynamic approach was extended. Besides, it was possible to incorporate the liquid volume fraction in the tabulated thermodynamics and predict the liquid penetration in all cases without any empirical coefficient tuning, being an alternative approach to Eulerian-Lagragian simulation [63-64].

Fuel property comparison

Next, predictions obtained with the V0a and V1 surrogates are presented. As the results present similar behavior, the comparison for 1100K and 15.2kg/m^3, 1400K and 7.6kg/m^3 ambient condition will be omitted and only the 900K and 22.8kg/m^3 case is discussed in detail.

Figure 8 shows the vapor penetration as a function of time. The multi-component surrogates (V0a, V1) present slightly higher penetration rate in comparison to the single component (*n*-dodecane) fuel. The multi-component surrogates have some components with a boiling point lower than *n*-dodecane (489.0K) as 1,24-trimethylbenzeno (442.6K) and n-butycyclohexane (456.2k), that could impact on an earlier fuel evaporation. However, they represent less than 8% of the molar fraction. So, it is not possible to assume that the boiling point has a governing role in the vapor penetration base on this absolute difference. The same conclusion is also applicable for the fuel density and the vapor penetration. There is not a clear correlation for the narrow liquid density range (730-828kg/m^3) analyzed here. This same conclusion is found in previous studies[65-66].

Figure 9 illustrates the fuel mixture fraction profile for the surrogates. The V0a and V1 present the same fuel distribution in all axial range, as shown by the overlapping curves. This behavior is expected since their composition palette aims to match the composition characteristics of the same target fuel, no. 2-D S15 diesel [14]. The multi-component surrogates present a higher concentration at the central region of the jet, between 0-2mm radius, beyond the 2mm redial position the distribution is practically the same for all three fuels.

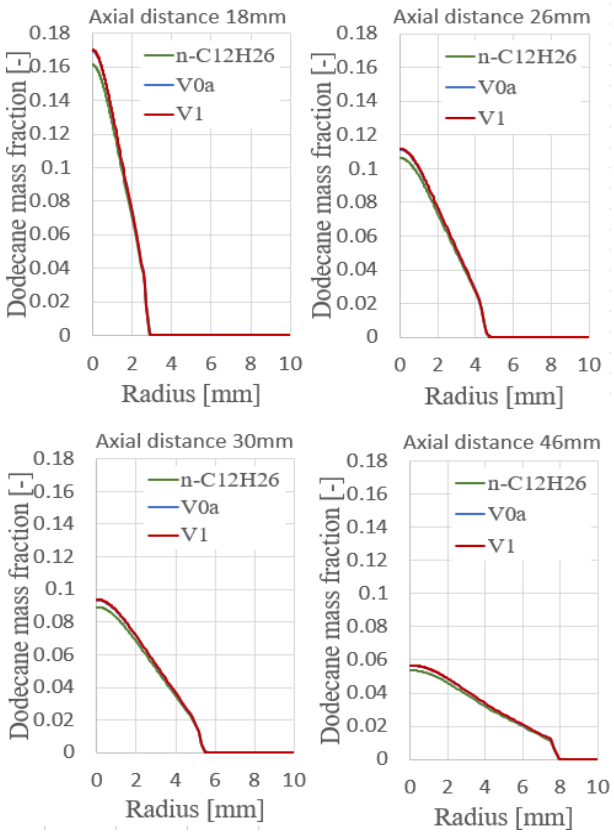

Figure 9: Radial mixture fraction profiles for n-dodecane, V0a and V1 at different distances from the nozzle at 900K and 22.8kg/m3 ambient condition.

In contrast, Figure 10 shows the temporal variation of liquid penetration, where the difference imposed due to the surrogate selection are clear. Several factors justify this difference. The fuel with low-boiling point, as *n*-dodecane, evaporates fast and its liquid penetration is lower. For the multi-component surrogates, more than 65% of the molar fraction present higher boiling point components in comparison to *n*-dodecane; the latter is having a smaller liquid penetration due to higher volatility. The *n*-dodecane liquid penetration is on average 1mm lower than the multi-component V0a and V1.

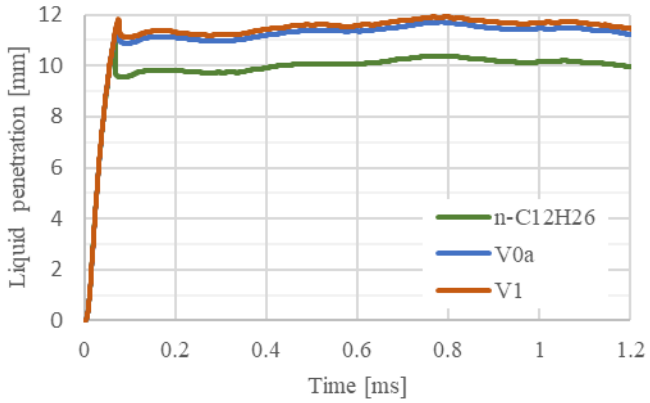

Figure 10: Liquid penetration for n-dodecane, V0a and V1 at 900K and 22.8kg/m3 ambient condition.

Another direct association can be observed between the fuel density and liquid length, as illustrated in Figure 11, where a linear correlation can be observed on the cases simulated. The V1 present the higher density (828Kg/m^3) and the longest liquid length, 11.9mm, followed by V0a (828Kg/m^3 and 11.7mm) and *n*-dodecane (730Kg/m^3 and 10.4mm).

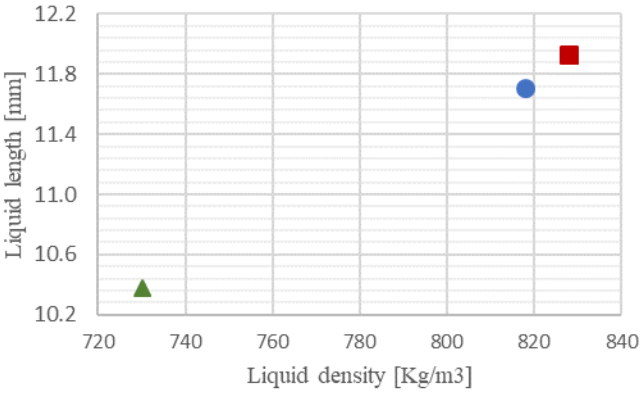

Figure 11: Fuel density and liquid length correlation at 900k/60bar ambient condition.

These absolute differences are relevant since the precise liquid penetration prediction is an important factor for direct-injection diesel engine development. When the liquid length reaches the piston head and/or cylinder liner wall, a fuel film may form that could combust at different time from the main combustion, increasing the soot and NOx emissions. The liquid impingement may also result to other negatives effects as higher hydrocarbon and carbon monoxide emissions, increase piston-wall friction and engine-component wear [67]. It is also mentioned that the liquid length may be affected by other fuels properties such as viscosity, heat of vaporization, vapor pressure and latent heat [65], especially for the multi-component surrogates.

The predicted mean velocity at spray centerline is illustrated in Figure 12. Until approximately 3mm axial distance, the centerline velocity increases, as *n*-dodecane tends to be more accelerated than the multi-component surrogates. This velocity increase is followed by a deceleration, which is more pronounced for *n*-dodecane, until all surrogates decelerate to the same velocity value.

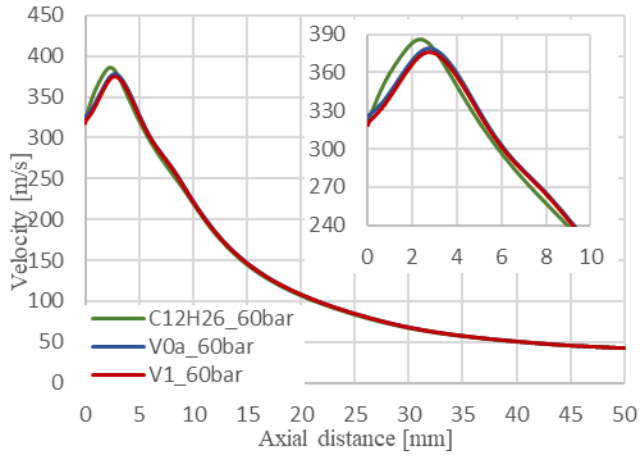

Figure 12: Mean spray centerline velocity for n-dodecane, V0a and V1 at 900K and 22.8kg/m3 ambient condition.

Lastly, all surrogates present the same temperature at the spray centreline. As expected, the centerline temperature increases as function of the surrogate and nitrogen mixing.

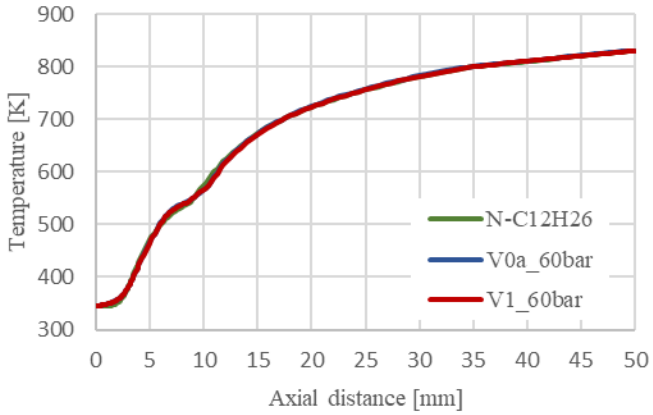

Figure 13: Temperature distribution along the jet central line at 900K and 22.8kg/m3 ambient condition.

Numerical extrapolation: penetration behavior

The numerical method allows exploration of the sole effect of fuel properties. One simulation was performed with V0a at 900K and 22.8kg/m^3 ambient condition. However, the *n*-dodecane mass flow rate profile was used instead of V0a mass flow rate profile as boundary condition.

As illustrated in Figure 2, the V0a mass flow rate is around 7.2% higher compared to *n*-dodecane mass flow rate at 60bar ambient pressure. Even though this extrapolation is not physically accurate, it is still interesting to analyze the sole effect of the thermodynamic properties of surrogates.

Figure 14 shows the vapor penetration and Figure 15 the liquid penetration as function of time. The green line represents the *n*-dodecane results, the blue line represents the V0a and the yellow line the V0a with *n*-dodecane mass flow rate profile as boundary condition, named as V0a – Extrapolation.

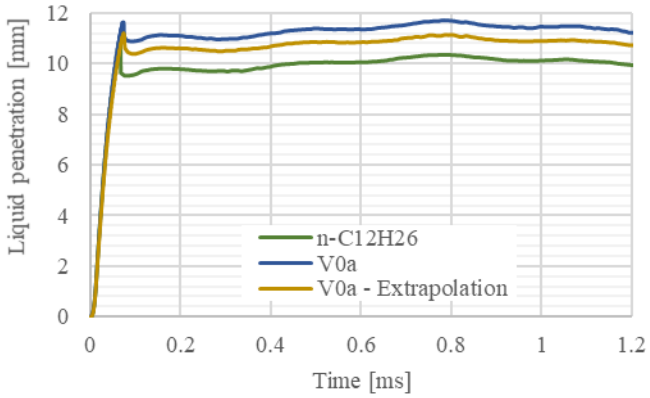

Figure 14: Vapor penetration for n-dodecane and V0a at 900K and 22.8kg/m3 ambient condition

As examined before, *n*-dodecane and V0a have the same behaviour for vapour penetration. However, V0a-Extrapolation presents a slightly lower vapor penetration. This difference makes clear the impact of fuel properties (*n*-dodecane and V0a-Extrapolation comparison) and boundary condition (V0a and V0a-Extrapolation comparison) on the results. At 1.0ms, the vapor penetration reaches 47.1mm for the n-dodecane, 47.5mm for the V0a and 45.5mm for the V0a-Extrapolation. The boundary condition has 4.20% relative difference (V0a and V0a-Extrapolation comparison) and the fuel properties 3.38% relative difference (n-dodecane and V0a-Extrapolation comparison).

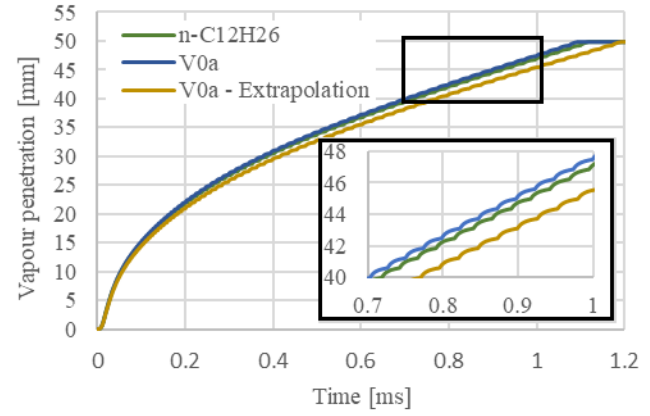

Figure 15: Liquid penetration for n-dodecane and V0a at 900K and 22.8kg/m3 ambient condition.

The difference is more relevant for the liquid penetration (Figure 15). Disregarding the initial liquid detachment, the maximum distance achieved for the three cases are: 10.4mm for the n-dodecane, 11.7mm for the V0a and 11.2mm for the V0a-Extrapolation. The fuel selection results to an 7.62% relative difference (*n*-dodecane and V0a-Extrapolation comparison) and the boundary condition on 4.65% relative difference (V0a and V0a-Extrapolation comparison).

Summary/Conclusions

In this work, three diesel surrogates were numerically compared using a tabulated thermodynamic modelling based on PC-SAFT EoS. The surrogates can be divided in two groups: one mono-component (n-dodecane) and two multi-component (V0a and V1). Both multi-component surrogates were formulated to match the compositional characteristics of the same target fuel, no. 2-D S15 diesel, which justifies the similar performance. The PC-SAFT EoS model can be applied to both types of surrogates. This modelling approach presents a considerable advantage due to the independence of tunable coefficients, a necessary practice in Eulerian-Lagragian modelling. All simulations were performed in non-reacting conditions. First, the ECN Spray A was validated in three target conditions, demonstrating the reliability and versatility of this method in complement to previous studies. Second, the different surrogates were compared aiming to understand their characteristics on fuel mixing, vapor and liquid penetrations. It was found that it is possible to associate the fuel density and boiling point with the liquid penetration, being directly proportional to these properties. In fact, the type of diesel surrogate can lead to a difference higher than 1mm for the maximum liquid penetration.

References

1. Wexler, P. Ed., Encyclopedia of Toxicology, S.C. Gad, 2014, pp. 115-118.
2. Galle J. and Verhelst, S., "Influence of Diesel Surrogates on the Behavior of Simplified Spray Models," Lecture Notes in Electrical Engibeeribg, vol. 189, pp. 361-374, 2013.
3. Folkson, R.,Ed., Alternative Fuels and Advanced Vehicle Technologies for Improved Environmental Performance, Woodhead Publishing, 2014, pp. 165-194.
4. Pitz, W. J. and Mueller, C. J., "Recent Progress in the Development of Diesel Surrogate Fuels," Progress in Energy and Combustion Science, vol. 37, no. 3, pp. 330-350, 2011.
5. Kundu, P. , Xu, C., Som, S., Temme, J. C. et al., "Implementation of multi-component diesel fuel surrogates and chemical kinetic mechanisms for engine combustion simulations," Transportation Engineering, 2021.
6. Som, S., Longman, D. E., Luo, Z., Plomer, M. et al., "Three Dimensional Simulations of Diesel Sprays Using n-Dodecane as a Surrogate," in Fall Technical Meeting of the Eastern States Section of the Combustion Institute, Connecticut, 2011.
7. Szymkowicz, P. and Benajes, J., "Development of a Diesel Surrogate Fuel Library," Fuel, vol. 222, pp. 21-34, 2018.
8. Mueller, C. J., Cannella, W. J., Bruno, T. J., Bunting, B. et al, “Methodology for Formulating Diesel Surrogate Fuels with Accurate Compositional, Ignition-Quality, and Volatility Characteristics,” Energy and Fuels, no. 26, p. 3284−3303, 2012.

9. Jamali, A., Purushothaman, K. and Ra, Y., "A combustion model for multi-component fuels based on relative reactivity and molecular structure," Fuel, 2021.
10. Pei, Y., Mehl, M., Liu, W., Lu, T. et al., "A Multicomponent Blend as a Diesel Fuel Surrogate for Compression Ignition Engine Applications," ASME, vol. 137, 2015.
11. Sun, X., Li, X., Huang, Z., Ju, D. et al., "Numerical Analysis on the Injection and Atomization Characteristics of Diesel Surrogates at Engine Conditions," SAE Technical Paper, 2017.
12. Qian, Y., Yu, L., Li, Z., Zhang, Y. et al., "A New Methodology for Diesel Surrogate Fuel Formulation: Bridging Fuel Fundamental Properties and Real Engine Combustion Characteristics," Energy, vol. 148, pp. 424-447, 2018.
13. Sun, X., Wang, M., Atilla, I., Feng, S., et al, "Development of a multi-component surrogate fuel model of marine diesel engine," Ocean Engineering, vol. 233, 2021.
14. Mueller, C. J., Cannella, W. J., Bays, J. T., Bruno, T. J., et al., "Diesel Surrogate Fuels for Engine Testing and Chemical-Kinetic Modeling: Compositions and Properties," Energy and Fuels, vol. 30, pp. 1445-1461, 2016.
15. Wensing, M., Vogel, T., and Götz, G., "Transition of diesel spray to a supercritical state under engine conditions," International Journal of Engine Research, vol. 17, no. 1, pp. 108-119, 2016.
16. Salvador, F. J., De la Morena, J., Martínez-López, J., and Jaramillo, D., "Assessment of compressibility effects on internal nozzle flow in diesel injectors at very high injection pressures," Energy Conversion and Management, pp. 221-230, 2017.
17. Crua, C., Manin, J., and Pickett, L. M., "On the transcritical mixing of fuels at diesel engine conditions," Fuel, vol. 208, pp. 535-548, 2017.
18. Soave, G., "Equilibrium constants from a modified Redlich-Kwong equation of state," Chemical Engineering Science, vol. 27, pp. 1197-1203, 1972.
19. Peng, D. and Robinson, D. B.,"New Two-Constant Equation of State," Industrial & Engineering Chemistry Fundamentals , vol. 15, no. 1, pp. 59-64, 1976.
20. S. Yang, P. Yi and C. Habchi, "Real-fluid injection modeling and LES simulation of the ECN Spray A injector using a fully compressible two-phase flow approach," International Journal of Multiphase Flow, vol. 122, p. 103145, 2020.
21. C. Tsonopoulos and J. L. Heidman, "From Redlich-Kwong to the present," Fluid Phase Equilibria, vol. 24, pp. 1-23, 1985.
22. Koukouvinis, P., Vidal-Roncero, A., Rodriguez, C., Gavaises, M. et al., "High pressure/high temperature multiphase simulations of dodecane injection to nitrogen: Application on ECN Spray-A," Fuel, vol. 275, 2020.
23. Ningegowda, B. M., Rahantamialisoa, F. N., Pandal, A., Jasak, H. at al., "Numerical Modeling of Transcritical and Supercritical Fuel Injections Using a Multi-Component Two-Phase Flow Model," Energies, vol. 13, no. 21, 2020.
24. Rokni, H. B., Moore, J. D. and Gavaises, M., "Entropy-scaling based pseudo-component viscosity and thermal conductivity models for hydrocarbon mixtures and fuels containing iso- alkanes and two-ring saturates," Fuel, vol. 283, 2021.
25. Rowane, A. J., Gupta, A., Gavaises, M. and McHugh, M. A., "Experimental and modeling investigations of the interfacial tension of threedifferent diesel + nitrogen mixtures at high pressures and temperatures," Fuel, vol. 280, 2020.
26. Rowane, J., Mallepally, R. R., Gavaises M. and McHugh, M. A.,"Interfacial Tension of Isomers n-Hexadecane and 2,2,4,4,6,8,8-Heptamethylnonane with Nitrogen at High Pressures and Temperatures," Industrial & Engineering Chemistry Research, vol. 59, no. 19, pp. 9293-9299, 2020.
27. Rowane, J., Gupta, A., Gavaises, M. and McHugh, M. A., "Experimental and modeling investigations of the phase behavior and densities of diesel + nitrogen mixtures," Fuel, vol. 265, 2020.
28. Rowane, J., Gavaises, M. and McHugh, M. A., "Vapor-liquid equilibria and mixture densities for 2,2,4,4,6,8,8-heptamethylnonane + N2 and n-hexadecane + N2 binary mixtures up to 535 K and 135 MPa," Fluid Phase Equilibria, vol. 506, 2020.
29. Rowane, J., Babu, V. M., Rokni, H. B., Moore, J. D. et al., "Effect of Composition, Temperature, and Pressure on the Viscosities and Densities of Three Diesel Fuels," Journal of Chemical & Engineering Data, vol. 64, no. 12, pp. 5529-5547, 2019.
30. Rokni, H. B., Moore, J. D., Gupta, A., McHugh, M. A. et al., "General method for prediction of thermal conductivity for well-characterized hydrocarbon mixtures and fuels up to extreme conditions using entropy scaling," FueL, vol. 245, 2019.
31. Rowane, A. J., Mallepally, R. R., Gupta, A., Gavaises, M. et al., "High-Temperature, High-Pressure Viscosities and Densities of n-Hexadecane, 2,2,4,4,6,8,8-Heptamethylnonane, and Squalane Measured Using a Universal Calibration for a Rolling-Ball Viscometer/Densimeter," Industrial & Engineering Chemistry Research, vol. 58, no. 10, pp. 4303-4316, 2019.
32. Rokni, H. B., Moore, J. D., Gupta, A., McHugh, M. A. et al., "Entropy scaling based viscosity predictions for hydrocarbon mixtures and diesel fuels up to extreme conditions," Fuel, vol. 241, p. 1377–1390, 2019.
33. Rokni, H. B., Gupta, A., Moore, J. D., McHugh, M. A. et al., "Purely predictive method for density, compressibility, and expansivity for hydrocarbon mixtures and diesel and jet fuels up to high temperatures and pressures," Fuel, vol. 236, pp. 1377-1390, 2019.
34. Chapman, W. G., Gubbins, K. E., Jackson, G. and Radosz, M., "SAFT: Equation-of-State Sollution model for associating fluids," Fluid Phase Equilibria, vol. 52, pp. 31-38, 1989.
35. Gross, J. and Sadowski, G., "Perturbed-chain SAFT:An equation of state based on a perturbation theory for chain molecules," Industrial & Engineering Chemistry Research, vol. 40, no. 4, pp. 1244-1260, 2001.
36. Perez, A.G., Coquelet, C., Paricaud, P. and Chapoy, A.,"Comparative study of vapour-liquid equilibrium and density modelling of mixtures related to carbon capture and storage with the SRK, PR, PC-SAFT and SAFT-VR Mie equations of state for industrial uses," Fluid Phase Equilibria, 2017.
37. Diamantonis, N. I., Boulougouris, G. C., Mansoor, E., Tsangaris, D. M. et al., "Evaluation of Cubic, SAFT, and PC-SAFT Equations of State for the Vapor−Liquid Equilibrium Modeling of CO2 Mixtures with Other Gases," Industrial & Engineering Chemistry Research, vol. 52, pp. 3933-3942, 2013.

38. Vidal, A., Koukouvinis, P. and Gavaises, M., "Vapor-liquid equilibrium calculations at specified composition, density and temperature with the perturbed chain statistical associating fluid theory (PC-SAFT) equation of state," Fluid Phase Equilibria, vol. 521, p. 112661, 2020.
39. Vidal, Rodriguez, C., Koukouvinis, P., Gavaises, M. et al., "Modelling of Diesel fuel properties through its surrogates using Perturbed-Chain, Statistical Associating Fluid Theory," International J of Engine Research, vol. 21, no. 7, pp. 1118-1133, 2020.
40. Wilhelmsen, O., Aasen, A., Skaugen, G., Aursand, P. et al., "Thermodynamic Modeling with Equations of State: Present Challenges with Established Methods," Industrial & Engineering Chemistry Research, vol. 56, pp. 3503-3515, 2017.
41. Kyriazis, N., Koukouvinis, P., and Gavaises, M., "Numerical investigation of bubble dynamics using tabulated data," International Journal of Multiphase Flow, 2017.
42. A. Rubino, M. Pini, M. Kosec, S. Vitale and P. Coluna, "A look-up table method based on unstructured grids and its application to non-ideal compressible fluid dynamic simulations," Journal of Computational Science, vol. 28, pp. 70-77, 2018.
43. C.Rodriguez, A.Vidal, P.Koukouvinis, M.Gavaises and M.A.McHugh, "Simulation of transcritical fluid jets using the PC-SAFT EoS," Journal of Computational Physics, vol. 374, p. 444–468, 2018.
44. Koukouvinis, P., Vidal-Roncero, A., Rodriguez, C., Gavaises, M. et al., "Enhancing the predictive capabilities for high P/T fuel sprays; non-ideal thermodynamic modelling using PC-SAFT," 2020.
45. Koukouvinis, P., Rodriguez, C., Hwang, J., Karathanassis, I. et al., "Machine Learning and transcritical sprays: A demonstration study of their potential in ECN Spray-A," International Journal of Engine Research, p. 1–17, 2021.
46. Vidal, A., Kolovos, K., Gold, M. R., Pearson, R. J. et al., "Preferential cavitation and friction-induced heating of multi-component Diesel fuel surrogates up to 450MPa," International Journal of Heat and Mass Transfer, vol. 166, p. 120744, 2021.
47. Inc., ANSYS Fluent v19.1 Manual, 2018.
48. Tahery, R. and Modarress, H., "Lennard-jones energy parameter for pure fluids from scaled particle theoory," Iranian Journal of Chemistry and Chemical Engineering, vol. 26, no. 2, pp. 1-8, 2007.
49. Wei, H., Chen, X., Zhao, W., Zhou, L. et al., "Effects of the turbulence model and the spray model on predictions of the n-heptane jet fuel-air rmixing and the ignition characteristics with a reduced chemistry mechanism," Proceedings of the Institution of Mechanical Engineers, Part D: Journal of Automobile Engineering, vol. 231, no. 14, pp. 1877-1888, 2017.
50. Lotgering-Lin, O. and Gross, J., "A group contribution method for viscosities based on entropy scaling using the perturbed-chain polar statistical associating fluid theory," Industrial & Engineering Chemistry Research, vol. 54, no. 32, p. 7942–7952, 2015.
51. Hopp, M. and Gross, J., "Thermal Conductivity from Entropy Scaling: A Group-Contribution," Industrial & Engineering Chemistry Research, vol. 58, no. 44, p. 20441–20449, 2019.
52. Michelsen, M. L. and Mollerrup, J. M., in Thermodynamic Models: Fundamentals & Computational Aspects, Tie-Line Publications, 2007, pp. 231-238.
53. Justo-García, D. N., García-Sánchez, F. and Romero-Martínez, A., "Isothermal Multiphase Flash Calculations with the PC-SAFT Equation of State," in Recent Developments in Physical Chemistry, 3rd Mexican Meeting on Mathematical and Experimental Physics, 2008.
54. "Engine Combustion Network, “Spray A geometry," [Online]. Available: https://ecn.sandia.gov/diesel-spray-combustion/target-condition/spray-a-nozzle-geometry/.
55. Koukouvinis, P., Vidal-Roncero, A., Rodriguez, C., Gavaises, M. et al., "Enhancing the predictive capabilities for high P/T fuel sprays; non-ideal thermodynamic modelling using PC-SAFT," ERCOFTAC Bulletin 89, 2020.
56. "Engine Combustion Network, "Diesel Data Search page"," [Online]. Available: https://ecn.sandia.gov/ecn-data-search/.
57. Roncero, A. V.,"Numerical modelling of multiphase diesel fuel properties using the PC-SAFT equation of state and its effect on nozzle flow and cavtation under extreme pressurisation," Thesis - City, University of London, 2020.
58. U.S. Departament of Commerce, "NIST Chemistry WebBook," [Online]. Available: https://webbook.nist.gov/cgi/cbook.cgi?ID=C112403&Mask=4. [Accessed 07 2021].
59. Lemmon, E. W., Bell, I. H., Huber, M. L. and McLinden, M. O., NIST Standard Reference Database 23: Reference Fluid Thermodynamic and Transport Properties-REFPROP, Version 10.0, National Institute of Standards and Technology, 2018.
60. "CMT, Virtual Injection Rate Generator," [Online]. Available: https://www.cmt.upv.es/ECN03.aspx.
61. Engine Combustion Network, "ECN - Diesel data search page," [Online]. Available: https://ecn.sandia.gov/ecn-data-search/. [Accessed july 2021].
62. Matheis, J. and Hickel, S., "Multi-component vapor-liquid equilibrium model for LES of high-pressure fuel injection and application to ECN Spray A," International Journal of Multiphase Flow, vol. 99, pp. 294-311, 2018.
63. Wehrfritz, A., Vuorinen, V., Kaario, O. and Larmi, M., "Large Eddy Simulation of High Velocity Fuel Sprays: Studying mesh resolution and breakup model effects for spray A," Atomization and Sprays, vol. 23, no. 5, pp. 4199-442, 2013.
64. Gadalla, M., Kannan, J., Tekgül, B., Karimkashi, S. et al., "Large-Eddy Simulation of ECN Spray A: Sensitivity Study on Modeling Assumptions," Energy, 2020.
65. Kaario, O. T., Vuorinen, V., Kahila, H., Im, H. et al., "The effect of fuel on high velocity evaporating fuel sprays: Large-Eddy simulation of Spray A with various fuels," International J of Engine Research, vol. 21, no. 1, pp. 26-42, 2020.
66. Kook, S. and Pickett, L. M., "Liquid length and vapor penetration of conventional, Fischer–Tropsch, coal-derived, and surrogate fuel sprays at high-temperature and high-pressure ambient conditions," Fuel, pp. 539-548, 2012.
67. Dumitrescu, E., Polonowski, C. J., Fisher, B. T., Lilik, G. K. et al., "Diesel Fuel Property Effects on In-Cylinder Liquid Penetration Length: Impact on Smoke Emissions and Equivalence Ratio Estimates at the Flame LiftOff Length," Energy and Fuels, vol. 29, no. 11, pp. 7689-7704, 2015.

Contact Information

Marilia G. J. Vaz
CITY, University of London
International Institute for Cavitation Research and Thermo-Fluids Research Centre
Northampton Square
London EC1V 0HB - United Kingdom
Marilia.Justino-Vaz@city.ac.uk

Acknowledgments

This work has received funding from the European Union's Horizon 2020 research and innovation programme under the Marie Sklodowska-Curie grant agreement No 861002

Definitions/Abbreviations

BFGS	Broyden-Fletcher-Goldfarb-Shanno
CFD	Computational fluid dynamics
ECN	Engine Combustion Network
EoS	Equation of state
HMN	Heptamethylnonane
HPHT	High pressure and high temperature
PC-SAFT	Perturbed Chain Statistical Associating Fluid Theory
VLE	Vapor Liquid Equilibrium

Appendix

The Appendix is one-column. If you have an appendix in your document, you will need to insert a continuous page break and set the columns to one. If you do not have an appendix in your document, this paragraph can be ignored and the heading and section break deleted.